VOL. 18, NO. 10, MAY 2023 ISSN 1819-6608
ARPN Journal of Engineering and Applied Sciences
©2006-2023 Asian Research Publishing Network (ARPN). All rights reserved.
www.arpnjournals.com

CHROMIUM DOPED IRON OXIDE NANOPARTICLES AND PHYSICAL PROPERTIES PREPARED FROM LOGAS NATURAL SAND AND THEIR APPLICATION IN PHOTO-FENTON DEGRADATION OF METHYLENE BLUE DYE

Erwin Amiruddin[1], Salomo Sinuraya[1], Amir Awaluddin[2], Martha Rianna[3], Heri Hadianto[4], Muhammad Rizki[4], Novia Magdalena Purba[4] and Indah Tamara Sitorus[4]
[1]Department of Physics, Faculty of Mathematics and Natural Sciences, Riau University, Pekanbaru, Indonesia
[2]Department of Chemistry, Faculty of Mathematics and Natural Sciences, Riau University, Pekanbaru, Indonesia
[3]Department of Physics, Faculty of Mathematics and Natural Sciences, Universitas Sumatera Utara, Medan, Indonesia
[4]Magnetic Laboratory, Faculty of Mathematics and Natural Sciences, Riau University, Pekanbaru, Indonesia
E-Mail: erwin.amiruddin@lecturer.unri.ac.id

ABSTRACT

Chromium-doped iron oxide nanoparticles were prepared by ball milling method. The iron oxide nanoparticles were extracted from Logas-Kuansing natural sand. The structural, magnetic, morphological and optical properties of these nanoparticles were investigated using X-ray diffraction, vibration sample magnetometer (VSM), scanning electron microscopy (SEM) and UV-Vis spectroscopy. The X-ray diffraction revealed that undoped and chromium doped samples are hexagonal structure however, the crystalline size decreases from 38 nm to 35, 32, 30, 28 nm for the undoped and chromium doped samples with concentration of 5, 10, 15 and 20 wt.%, respectively. Magnetic properties have been analyzed by hysteresis loops using VSM. The coercivity, saturation magnetization and remanence magnetization have been found in the range of 138-254 Oe, 0.820-0.621 emu/g and 0.163-0.123 emu/g, respectively. Particle shape and size have been examined by SEM. The SEM image confirmed that the size of chromium-doped iron oxide particles is in the range of nanometer particles. The optical band gap was estimated using the Tuch relation and it decreases from 2.07, 2.01, 1.97, 1,95 and 1.93 eV for undoped and 5, 10, 15 and 20 wt.% chromium doped iron oxide nanoparticles, respectively. The Photo Fenton degradation of methylene blue dye under visible light irradiation increases with degradation percentages 98.69 and 99.06% for chromium concentration of 10 and 20 wt.%, respectively, as compared to that of 98.27% for undoped iron oxide nanoparticles. This work suggests that the prepared iron oxide nanoparticles are attractive photo Fenton catalysts for the degradation of methylene blue in the water.

Keywords: logas natural sand, ball milling, photo-fenton degradation, chromium doped iron oxide, methylene blue.

Manuscript Received 6 February 2023; Revised 16 July 2023; Published 25 July 2023

INTRODUCTION

Nowadays, metal oxide materials in nanometer size are finding great interest not only for their fundamental scientific interest but also for their many technological applications, such as magnetic devices, sensors, and lithium ion batteries [1-3]. Among the various types of metal oxides, the iron oxide such as α-Fe_2O_3 is considered to be one of the most important and promising oxides due to their many technological applications started from catalysts [4] to biomedical applications [5, 6] and environmental remediation [7]. In the present investigation, preparation of iron oxide (α-Fe_2O_3) nanoparticles from natural sand [8] were done using mechanical milling method and subjected to structural, magnetic and morphological properties. There are several methods to prepare iron oxide nanoparticles including sol-ge[l] [9], hydrothermal [10], laser pyrolysis, [11] and ball milling [12-14]. However, the simplest way to prepare iron oxide nanoparticles is ball milling method [15]. In this method initially larger grain sizes of the sample are reduced to nanometer scale particles by mechanical means. The advantage of using this method is simple, efficient, high yield and low cost compared to other methods. Previous researchers [15, 16] have used ball milling method to produce magnetic iron oxide nanoparticles. For example researchers, [16] used ball milling method to prepare 39.2 nm α- Fe_2O_3 nanoparticles directly from Logas natural sand and found that the α-Fe_2O_3 nanoparticles has a hexagonal structure. Magnetic properties, phase and morphology of the obtained particles are depended on time, speed and types of milled balls [15]. One of the most important parameters for controlling the magnetic properties of magnetic iron oxide nanoparticles is the size of the particles. However, development of a simple, reliable, and low cost methodology to prepare magnetic iron oxide nanoparticles with controllable size and size distribution remains a challenging task for researchers.

Fast growing industry especially textile industry can cause industrial waste such as dyes that spread into water bodies such rivers or lakes. As a result, water pollution is one of serious environmental problems [17]. This dye in water has to be removed because it can harm living things [18]. Many methods have been developed to remove dyes from water [19], but the photocatalyst degradation method is a fast growing method because it is simple, cheap, effective, solar energy as input and cleans [20]. In this method, electron-hole pairs can be generated

©2006-2023 Asian Research Publishing Network (ARPN). All rights reserved.

in iron oxide under visible light irradiation followed by generation of active OH radicals. These OH radicals degrade organic pollutants such as dyes.

According to previous researchers [21], when transition metal elements doped into iron oxide nanoparticles, they alter the structural properties of that nanoparticles. Moreover, doping methodology and selection of doped transition metal influence the photocatalytic process. As it is known that the mechanism of the photocatalytic process is based on the number of electron-hole pairs produced through band gap radiation [22]. The main challenge for α-Fe_2O_3nanoparticles to be used as photocatalysts with high efficiency is the need to increase the charge separation of α-Fe_2O_3nanoparticles and their photocatalytic efficiency [23]. One of the ways to increase photonic efficiency and increase the charge separation of the catalyst is through doping α-Fe_2O_3nanoparticles with transition metals [24]. Several researchers [25] reported that the catalytic activity of iron oxide was increased by doping it with titanium, vanadium and chromium. The small energy band gap of α-Fe_2O_3nanoparticles not only increases the absorption of visible light but also creates electron-hole pairs thereby increasing the efficiency of photocatalytic [26]. The performance of α-Fe_2O_3nanoparticles as a photocatalyst depends on its magnetic properties, structure and morphology [27]. The small size of α-Fe_2O_3nanoparticles has a carrier charge with a short path to reach the surface. In this paper, we have investigated the magnetic, structural, morphological and optical properties of undoped and chromium doped iron oxide nanoparticles prepared from natural sand from Logas, Kuansing District, Riau Province using ball-milling method and their application in photo-Fenton degradation of methylene blue dye.

EXPERIMENTAL PROCEDURE

Raw Material and Chemical

Raw material used for preparing α-Fe_2O_3 nanoparticles is natural sands collected from Logas village-Kuansing District Riau Province. The chemical used for doping the α-Fe_2O_3nanoparticles is chromium with purity of 99.99%. Methylene blue dye was used as a pollution model for photo-Fenton application.

Preparation of Undoped and Chromium Doped Iron Oxide Nanoparticles

Prior to ball milling process, Logas natural sand was processed using iron sand separator (ISS) for reducing the amount of non-iron oxide particles in the samples. The product of ISS was then milled using 2 stage ball milling. In the first and second stage, the milling was carried out for 50 hours. The iron oxide non iron oxide particles were separated using NdFeB magnet for the product of each stage. The product of ball milling was divided into 5 parts with the same amount of weight. Each of these products was milled together with chromium as a dopant concentration of 0, 5, 10 and 15 % for 20 hours. Magnetic, structural, morphological and optical properties of the iron oxide nanoparticles before and after doping were analyzedusing vibration sample magnetometer (VSM), X-Ray Diffraction (XRD) scanning electron microscope (SEM) and UV-Vis Spectrometer. The concentration of the samples before and after being chromium doped was obtained using X- Ray Fluorescence Spectrometer (XRF).

Degradation of Methylene Blue

The photo-Fenton degradation of methylene blue solution (50 ppm) was carried out under visible-light irradiation using a 160 W mercury lamp at room temperature. In this experiment, 1.0 g of undoped and chromium doped iron oxide nanoparticles (catalyst) was added in 25 mL of 50 ppm methylene blue dye solution and stirred continuously for 30 min in the dark room to achieve adsorption equilibrium. The reaction was initiated by the addition of hydrogen peroxide (H_2O_2). Then, the dye solution inside the cuvette was stirred continuously throughout the experiment under 160 W Mercury lamp source and 10mL of solution was collected at regular 20 minutes time intervals to monitor the degradation process. The effects of undoped and chromium doped iron oxide nanoparticles on methylene blue degradation were evaluated by UV-Vis spectrophotometry.

RESULTS AND DISCUSSIONS

Structural Analysis

The XRD diffraction patternsof undoped and chromium doped iron oxide (α-Fe_2O_3) nanoparticles at different concentration are shown in Figure-1. The pattern was confirmed using X-Ray Diffractometer Philip equipped with Cu Kα radiation of wavelength 1.5405 Å. The diffraction pattern of undoped iron oxide nanoparticles indicates the diffraction peaks angle at 23.85°, 32.64°, 35.25°, 40.36°, 48.82°, 53.51°, 56.25°, 61.82° and 63.36° which can be indexed as (012), (104), (110), (113), (024), (116), (122), (214) and (300) crystal planes, respectively. These peak positions correspond to the standard Bragg positions of hexagonalα-Fe_2O_3[28] which is in good agreement with the JCPDS No. 89-8103. The average crystallite sizes estimated using Scherrer's formula[29] for the undoped iron oxide nanoparticles were found to be 38, 35, 32, 30, 28 nm for the chromium doping concentration of 0, 5, 10, 15 and 20 wt.%, respectively. The size decreases with increasing chromium content. Moreover, the intensity of the diffraction peaks are found to increase indicating the reducing of crystallitesize with chromium doping. The XRD patterns confirmed also the presence of one additional diffraction peak, namely at 2θ= 44.25° in the chromium doped samples. This low intensity diffraction peak shown in Figure-1 (b), (c), (d) and (e) indicated the presence of metallic chromium nanoparticles in the sample. Hence, the existence of diffraction peaks related to the chromium and hematite nanoparticles showed successful ball milling method to form hematite nickel nanoparticles. As the content of chromium nanoparticles increases, the (110) peak intensity was found to increase as clearly observed in Figure-1.

©2006-2023 Asian Research Publishing Network (ARPN). All rights reserved.

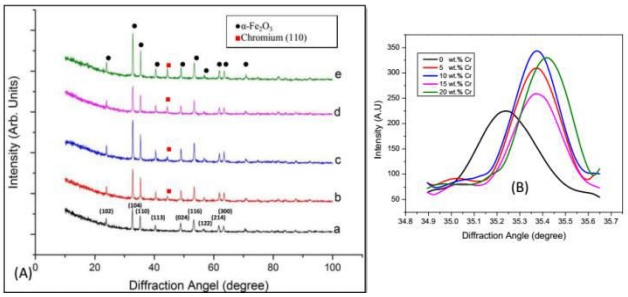

Figure-1. (A) XRD patterns of (a) undoped and chromium doped (b) 5 wt.% , (c) 10 wt.%, (d) 15 and (e) 20 wt.% α-Fe_2O_3 nanoparticles and (B) expanded diffraction angle of 35.0° – 35.6° showing shift of peak position to slightly higher angle.

Table-1. Concentration of iron oxide nanoparticles after milling 100 h and after chromium doping.

Name of Element	Concentration (%)	
	After milling 100 h	After 5 wt.% Cr doping
Si	1.376	0.987
Ti	36.309	32.500
Cr	0.080	7.758
Fe	57.317	54.204
others	4.918	4.551

Magnetic Properties

Figure-2 shows the magnetization (M) versus applied magnetic field (H) curve of the undoped and chromium doped (0, 5, 10, 15 and 20 wt.%) iron oxide nanoparticles. The measurement for the samples were carried out using vibration sample magnetometer (VSM) in the applied magnetic field of -20 kOe to +20 kOe. The saturation magnetization of the samples was calculated from a plot of magnetization versus applied magnetic field. As shown in Figure-2, the behavior of magnetization as a function of applied magnetic field is hysteretic with the magnetization of the iron oxide nanoparticles showing an increase with increasing the applied magnetic field and reach the saturation state under a high applied magnetic field of 20 kOe, which agrees with previous observations in earlier works[30]. From the figure it is clear that the samples exhibit ferromagnetic behavior. The saturation magnetization (Ms) and remanence magnetization (Mr) of undoped sample [Ms=0.82emu/g and Mr =0.163 emu/g], respectively decrease with increasing chromium content. However, the coercivity increases with increasing chromium content, due to crystallite size, and morphology of the samples as shown in Figure-3. Increasing amount of nonmagnetic doping concentration result more segregation among iron oxide nanoparticles consequently reduced the value of magnetization which was previously reported in literature [31].

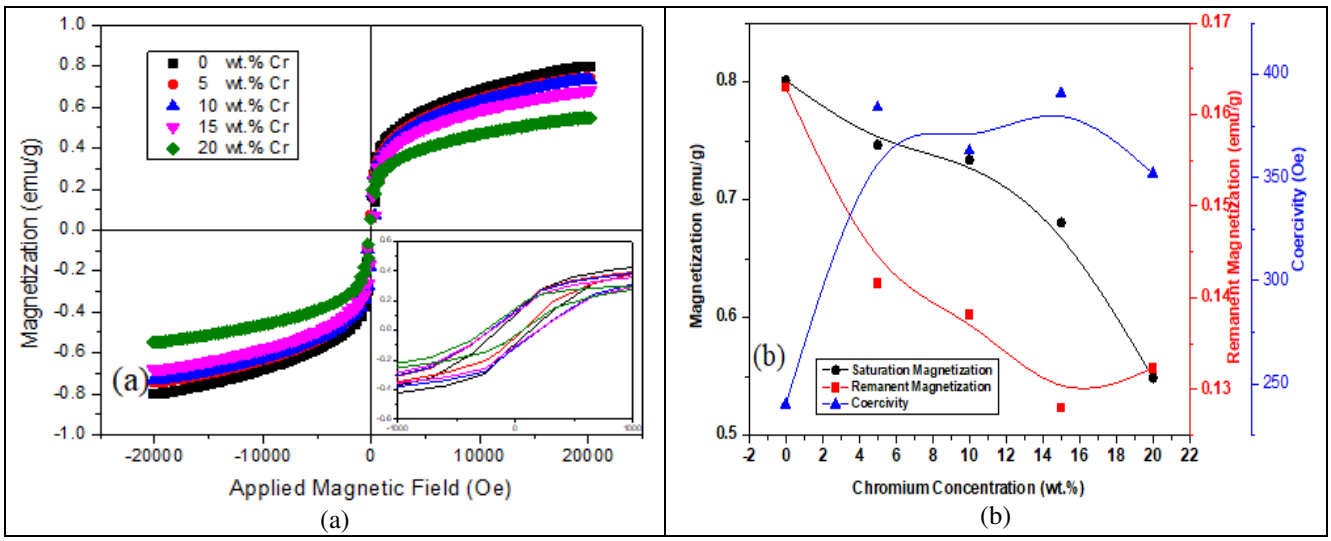

Figure-2. (a) Hysteresis curves of undoped and chromium doped iron oxide nanoparticles and the inset showing the enlarge loop of the samples and (b) magnetization, remanent magnetization and coercivity of the samples.

Morphological Properties

SEM images of undopedand chromium doped iron oxide nanoparticles at different concentrations are shown in Figure-3. Particle size of undoped sample Figure-3(a) is in the range of 0.1-10 µm and shows the growth of particles aggregate of smaller individual of different sizes. It can be noticed that undoped iron oxide nanoparticles were highly agglomerated with nonhomogeneous distribution. Formation of agglomerated particles arose due to the adhesive nature of the nanoparticles or more attractive force among iron oxide nanoparticles. In addition, the particles are irregular in shape and randomly organized. The average particle size estimated from these images for undoped α-Fe_2O_3 nanoparticles is roughly 1, 316 µm. SEM micrographs shown in Figure-3(b) and (c) clearly reveal that the particle size decreases with the increase of chromium content namely 10 wt.% and 20 wt.% and the same

©2006-2023 Asian Research Publishing Network (ARPN). All rights reserved.

behavior for Mg-Al doped iron oxide nanoparticles is reported by Rianna [32]. The average particle size decreases to 1,308µm and 0,856µm for the addition of chromium dopant with concentration of 10 and 20 wt.%, respectively and have more uniform particle sizes as compared to that for undoped sample. The chromium doped samples show less agglomeration due to a decrease in the particle size with smooth surface which may be attributed due to more separation among iron oxide nanoparticles and also it led to a decrease of magnetization of the samples.

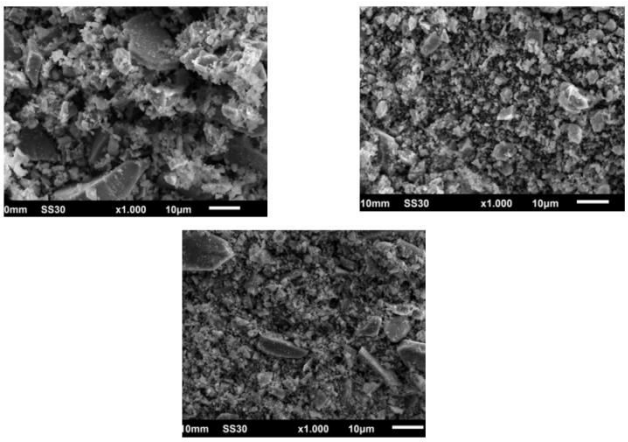

Figure-3. SEM images of (a) undoped iron oxide (b) 10 wt.% and (c) 20 wt.% chromium doped iron oxide nano particles.

Optical Properties

The effect of undoped and chromium doped (10 and 20 wt.%) on the optical properties of iron oxide nanoparticles was studied based on the optical absorbance measurements using UV-Vis spectrometer. The optical absorbance spectrum of undoped , 5, 10, 15 and 20 wt.% chromium iron oxide nanoparticles as a function of wavelength and optical band gap with average crystallite size and absorption peaks as a function of chromium concentration are shown in Figure-4(a) and 4(b), respectively. Previous researcher [33] showed that the absorbance characteristic of nanoparticles depends on particle size, band gap, structure, and surface roughness. A strong absorption at wavelength 217, 222, 218, 229 and 230 nm is observed in iron oxide nanoparticles for 0, 5, 10, 15 and 20 wt.% chromium doping, respectively. The strong absorption is found to shift towards higher wavelengths which associate with lower energies as chromium concentration increases and resulting more degradation of methylene blue.

The optical bang gap was obtained by plotting $(\alpha h\upsilon)^2$ versus the photon energy ($h\upsilon$) and by extrapolating the linear region ($\alpha = 0$). The optical band gap was estimated using the Tauc equation

$$\alpha h\nu = A\sqrt{E_g - h\nu} \quad \text{..... (1)}$$

where h is Planck constant, ν is frequency, α is the absorption coefficient and n - either 1/2 for a direct transition or 2 for an indirect transition. The direct band gap of iron oxide nanoparticles is shown in Figure-5. The results indicate that optical band gap calculated through UV-visible spectroscopy is decreased from 2.07 to 1.94 eV as the doping concentration of chromium is increased from 0 to 20 wt.%, respectively. Comparing our findings to those chromium doped iron oxide nanoparticles published earlier [34] the corresponding optical band-gap were in agreement. It is clear that chromium doping can narrow the optical band gap value of iron oxide nanoparticles. This result is consistent with that of published work [35]. The decrease in optical band gap could be due to the increase of densityof localized state in the conduction band [36]. Figure-5(b) shows the variation of the average crystallite size with optical band gap of chromium doped iron oxide nanoparticles. The band gap of undoped and chromium doped iron oxide nanoparticles decreases. Therefore, the crystallite size reduces the band gap of nanoparticles, which is in a good agreement with previous researcher [37]. This is due to the fact that with decrease in particle size and average crystallite size the band gap of the material decreases in which the valance band shifts to lower energies and the conduction band shifts to higher energies resulting more degradation of methylene blue.

©2006-2023 Asian Research Publishing Network (ARPN). All rights reserved.

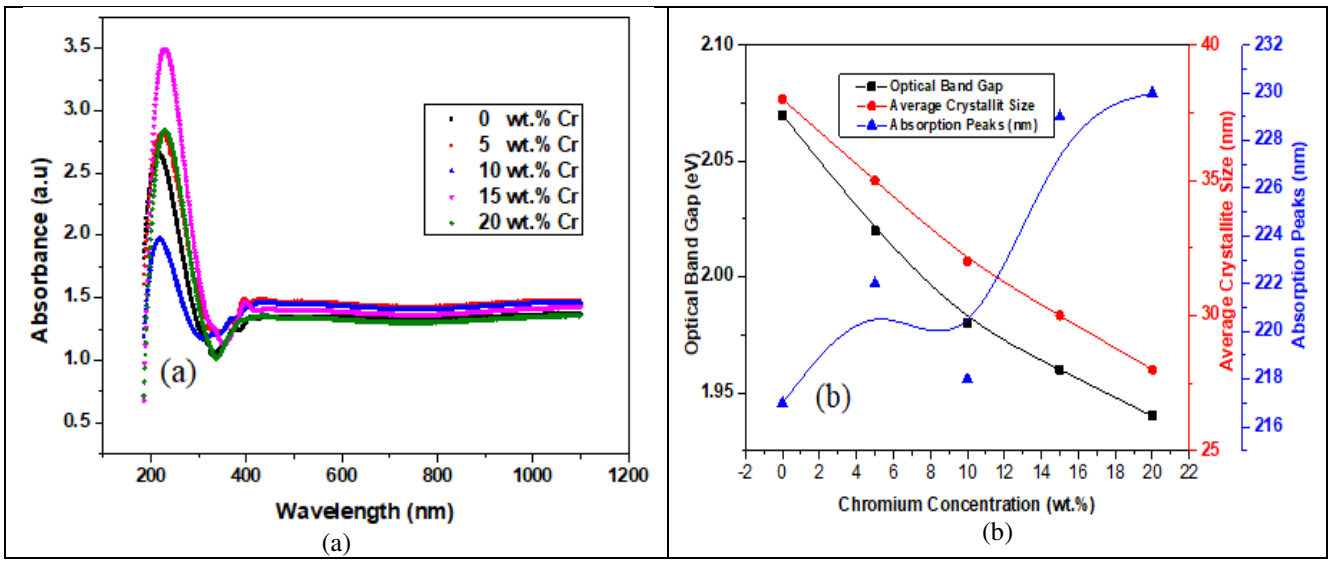

Figure-4. (a) Absorption spectra of undoped and chromium doped iron oxide nanoparticles at different doping weight percentages and (b) variation of crystallite size with opticalband gap and absorption peaks as a function of chromium concentration.

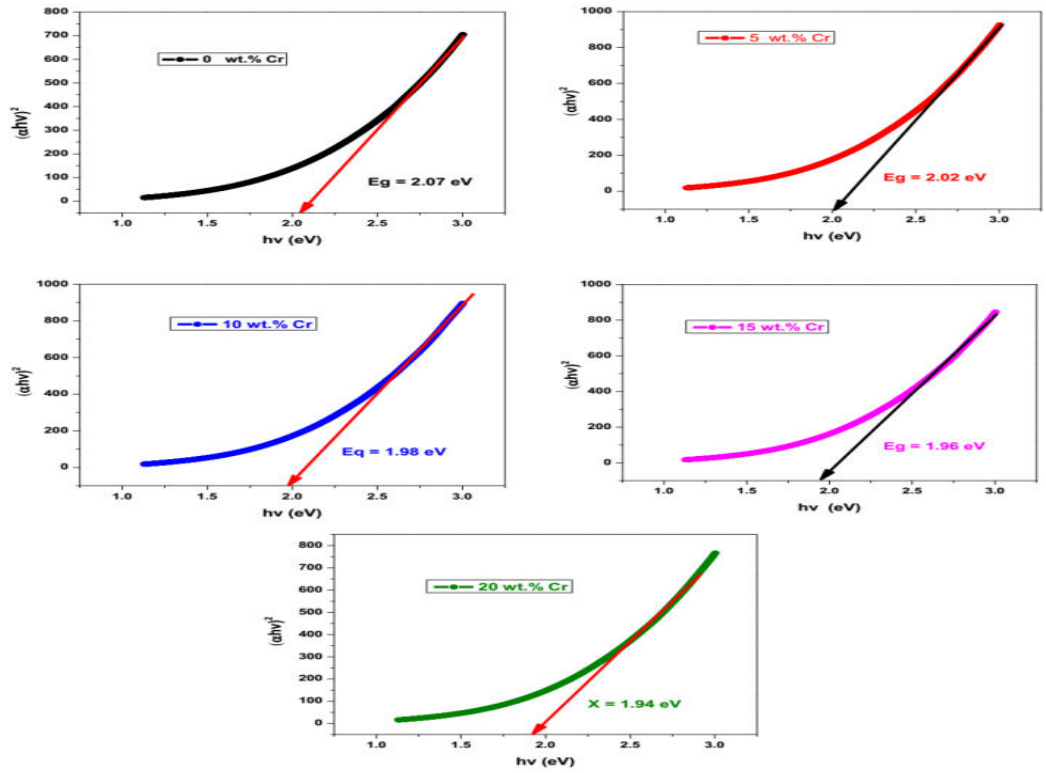

Figure-5. The optical band gap energy for undoped and chromium doped iron oxide nanoparticles at different doping weight percentage.

Photo-Fenton Activity of Iron Oxide Nanoparticles

The degradation of methylene blue (MB) with only iron oxide nanoparticles (NPs) and oxygen peroxide (H_2O_2) and with light and without oxygen peroxide (H_2O_2) was checked as indicated in Table-2. Previous researcher [15] showed similar results that degradation of MB is very low, but photosensitive in combination visible light and hydrogen peroxide [38]. The presence of H_2O_2 significantly improved the efficiency of MB degradation by 23.06% as compared to (MB + NPs + Light).

©2006-2023 Asian Research Publishing Network (ARPN). All rights reserved.

Table-2. Control experiments for MB degradation.

Experiment	MB+NPs	MB+H_2O_2	MB+NPs+Light	MB+NPs+H_2O_2+Light
MB Degradation (%)	9.8	9.6	76	99.06

Decomposition of methylene blue (MB) dye solution was monitored via percentage removal of MB dye according to following equation:

$$\% \text{ Degradation} = \left[\frac{C_o - C_t}{C_o}\right] x\ 100\% \quad \ldots\ldots\ldots\ldots (2)$$

where C_0 and C_t present initial concentration and concentration of MB in specific time, t. Figure-6 shows degradation of MB usingundoped and chromium doped iron oxide (α-Fe_2O_3) nanoparticles with inset picture shows the decolourization of MB dye of sample (a) to sample (f). It was observed that the increase in the chromium concentration from 0-10 wt.% showed a significant improvement in the efficiency of degradation by the system. Above 10 wt.% chromium concentration, the efficiency of degradation leveled off. This is due to the limited generation of hydroxyl radicals [39]. The degradation of methylene blue dye using chromium doped iron oxide nanoparticles as a catalyst is 99.06% after irradiation for 120 min. The plot of -ln(C_t/C_0) versus irradiation time for undoped and chromium doped iron oxide nanoparticles is shown in Figure-7. The slope of the plot -ln(C_t/C_0) with irradiation time results the rate constant in min^{-1} shown in Table-3.

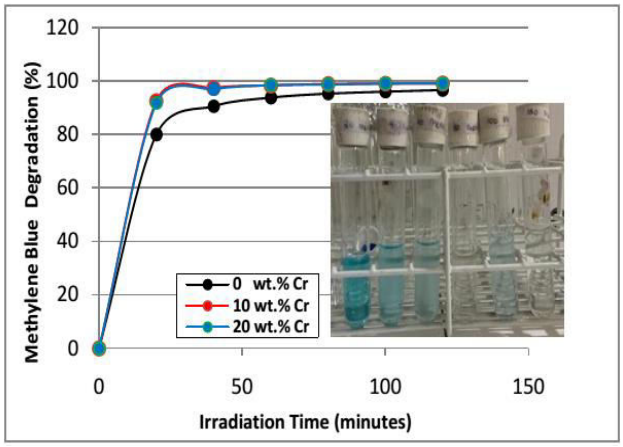

Figure-6. Degradation efficiency of MB as a function of irradiation time for different doping concentration of chromium. The inset picture shows the decolourization of MB dye of sample.

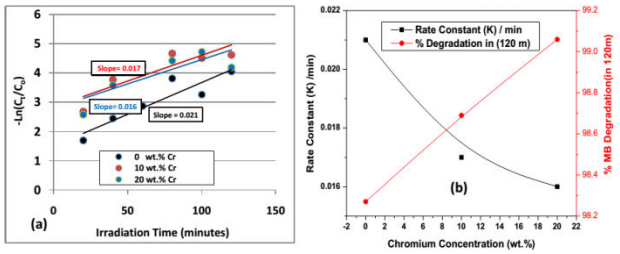

Figure-7. (a) Plot of $-Ln(C_t/C_o)$ with irradiation time of methylene blue dye and (b) rate constant and % MB degradation in 120 minutes using different concentrations of chromium.

CONCLUSIONS

Iron oxide (α-Fe_2O_3) nanoparticles with different chromium-doped weight percentages from 0 wt.% to 20 wt.% were successfully prepared using ball milling method to enhance photo-Fenton efficiency for methylene blue dye degradation under visible light irradiation. A structural characterization study using X-ray diffraction method revealed that all the samples are highly crystallized in the rhombohedral structure. The average crystalline size is found to decrease with increasing amounts of doping chromium. The existence of diffraction peaks related to the chromium and hematite nanoparticles showed successful ball milling method to form iron oxide chromium nanoparticles. The magnetic studies of the sample confirm the ferromagnetic nature of sample. The morphological properties of the samples showed the agglomeration of iron oxide nanoparticles were dominated for undoped sample. The optical band gap obtained from Tauc plot decreases with increasing chromium concentration. Photo Fenton degradation analysis shows iron oxide is a good catalyst for degradation of methylene blue dye under the illumination visible light and about 99% of methylene blue dye has been degraded in 120 minutes. Therefore, preparation of Iron oxide (α-Fe_2O_3) nanoparticles is excellent photo Fenton materials for water purification applications

ACKNOWLEDGMENTS

This work was financially supported by the Directorate General of Higher Education, Indonesian Ministry of Education, Culture, Research, and Technology 2022. The authors are grateful to Indonesian Sciences Institute (LIPI), for conducting the VSM and SEM measurements, Physics department UNP Padang for XRD measurements, and magnetic research members in Magnetism Laboratory FMIPA UNRI, for their assistance during sample collection and preparation.

©2006-2023 Asian Research Publishing Network (ARPN). All rights reserved.

REFERENCES

[1] Frey N. A., Peng S., Cheng K., Sun S. 2009. Magnetic nanoparticles: Synthesis, functionalization, and applications in bio imaging and magnetic energy storage. Chem. Soc. Rev. 38, pp. 2532-2542.

[2] C. Wang, L. Yin, L. Zhang, D. Xiang, R. Gao. 2010. Metal Oxide Gas Sensors: Sensitivity and Influencing Factors, Sensors: 10. DOI: 10.3390/s100302088.

[3] Morales J, Sanchez L. 1999. Electrochemical behaviour of SnO_2 doped with boron and indium in anodes for lithium secondary batteries. Solid State Ionics. Science Direct. 126: 219.

[4] Zhiqin Cao, Mingli Qin, Yueru Gu, Baorui Jia, Pengqi Chen, Xuanhui Qu. 2016. Synthesis and characterization of Sn doped hematite as visible light photocatalyst, Mater. Res. Bull. 77: 41-47.

[5] Colombo M., Carregal-Romero S., Casula M.F., Gutierez L., Morales M.P., Bohm I.B., Heverhagen J.T., Prosperi D., Parak W.J. 2012. Biological applications of magnetic nanoparticles. Chem. Soc. Rev. 41: 4306-4334.

[6] Singamaneni S., Bliznyuk V.N., Binek C., Tsymbal E.Y. 2011. Magnetic nanoparticles: Recent advances in synthesis, self-assembly and applications. J. Mater. Chem. 2011: 21: 16819-16845.

[7] Pegu R, Majumdar KJ, Talukdar DJ, Pratihar S. Oxalate capped iron nanomaterial: from methylene blue degradation to bis (indolyl) methane synthesis. Rsc. Advances. 4: 33446-33456.

[8] Erwin Amiruddin, SalomoSinuraya, Rahmondia N. Septiadi, Yanuar Hamzah, Amir Awaluddin, Loly A. Hardani, Fitri A. Lestari, Yessi Magdalena and Devi T. 2022. Gurning. A Systematic Study of The Structural and Magnetic Properties of Nickel Doped α-Fe_2O_3 Nanoparticles Prepared From Logas Natural Sand. ARPN Journal of Engineering and Applied Sciences: 17(14): 1408-1413.

[9] Chen Zahi S, Hashim M, Daud AR. 2007. Synthesis, magnetic properties and microstructure of Ni-Zn ferrite by sol-gel technique. J Magn. Magn. Mater. 308(2): 177-182.

[10] Tadica M, Panjan M, Damnjanovicc V, Milosevic I. 2014. Magnetic properties of hematite (α- Fe_2O_3) nanoparticles prepared by hydrothermal synthesis method. Appl. Surf Sci. 320: 183-7.

[11] Dumitrache F, Morjan I, Fleaca C, Badoi A, Manda G, Pop S, Marta DS, Huminic G, Huminic A, Vekas L, Daia C, Marinica O, Luculescu C, Niculescu AM. 2015. Highly magnetic Fe_2O_3 nanoparticles synthesized by laser pyrolysis used for biological and heattransfer applications. Appl Surf Sci. 336: 297-303.

[12] Amiruddin E and Prayitno A. 2019. The synthesis of magnetic nanoparticles from natural iron sand of Kata beach Pariaman West Sumatera using ball milling method as environmental material MATEC Web of Conferences. 276, 06014.

[13] A. Erwin, S. Salomo, P. Adhy, N. Utari, W. Ayu, Y. Wita and S. Nani. 2020. Magnetic iron oxide particles (Fe_3O_4) fabricated by ball milling for improving the environmental quality. IOP Conf. Series: Materials Science and Engineering. 845, 012051.

[14] S. Razavi-Tousi and J. Szpunar. 2015. Effect of ball size on steady state of aluminium powder and efficiency of impacts during milling. Powder Technology. 284: 149 158.

[15] Erwin Amiruddin, Amir Awaluddin, InnikeHariani, RibkaSihombing and RiskaAngraini. 2020. The Influence of Milling Ball Size on the Structural, Morphological and Catalytic Properties of Magnetite (Fe_3O_4) Nanoparticles toward Methylene Blue Degradation. Journal of Physics: Conference Series 1655. 012006 doi:10.1088/1742-6596/1655/1/012006

[16] Heri Hadianto, Erwin Amiruddin, RebiSeptiawan ,PutriVenera and ViviAprilia. 2020. Structural and Morphological Properties of Undoped and Manganese Doped Hematite Nanoparticles Prepared by Ball Milling Method. Journal of Physics: Conference Series 1655. 012013 doi:10.1088/1742-6596/1655/1/012013

[17] Dong W. *et al*. 2016. Preparation of secondary mesopores in mesoporousanatase-silica nanocomposites with unprecedented-high photocatalytic degradation performances. Adv. Funct. Mater. 26, 964-976.

[18] P. Movalli, O. Krone, D. Osborn, D. Pain. 2018. Monitoring contaminants, emerging infectious diseases and environmental change with raptors, and links to human health, Bird Study. 65: S96-S109.

©2006-2023 Asian Research Publishing Network (ARPN). All rights reserved.

[19] Nikta S. Moalej, SinaAhadi, SaeedSheibani. 2019. Photocatalytic degradation of methylene blue by 2 wt.% Fe doped TiO_2nanopowder under visible light irradiation. Journal of Ultrafine Grained and Nanostructured Materials. 52, pp. 133-141.

[20] S.N. Ahmed, W. Haider. 2018. Heterogeneous photocatalysis and its potential applications in water and wastewater treatment: a review, Nanotechnology. 29, 342001.

[21] Krishnan K M, Pakhomov A B, Bao Y, Blomqvist P, Chun Y and Griffin K. 2006. Nanomagnetism and spin electronics: materials, microstructure and novel properties Journal of Materials Science. 41: 793-815.

[22] A. A. Ismail, D. W. Bahnemann, L. Robben, M. Wark. 2010. Palladium doped porous titaniaphotocatalysts: Impact of mesoporous order and crystallinity, Chem. Mater. 22, 108-116.

[23] M. H. H. Mahamoud, A. A. Ismail, M. S. S. Sanad. 2012. Developing a cost-effective synthesis of iron oxide doped Titania photocatalysts loaded with palladium, platinum or silver nanoparticles, Chem. Eng. J. 187, 96-103.

[24] H. Liang, X. Jiang, W. Chen, S. Wang, B. Xu, Z. Wang. 2014. Ceram. Int. 40, 5653-5658.

[25] Qin DD, Li Y. L, Wang T, Li Y, Lu X Q, Gu J, Zhao, Y X, Song, Y M, Tao C L. 2015. Sn Doped Hematite Films as Photoanodes for Efficient Photoelectrochemical Water Oxidation, J.Mater. Chem. A 3(13): 6751-5.

[26] Hou J., Cheng H., Yang C., Takeda O. & Zhu H. 2015. Hierarchical carbon quantum dots/hydrogenated-γ-TaONheterojunctions for broad spectrum photocatalytic performance. Nano Energy. 18, 143-153.

[27] Liu Y., Yu, Y. X., Zhang W. D. 2012. Photoelectrochemical Properties of Ni-Doped Fe_2O_3Thin Films Prepared by Electrodeposition. Electrochim. Acta. 59, 121-127.

[28] K. Supattarasakda, K. Petcharoen, T. Permpool, A. Sirivat, W. Lerdwijitjarud. 2013. Control of hematite nanoparticle size and shape by the chemical precipitation method. Powder Technol. 249, 353-359.

[29] Achmad Maulana Soehada Sebayang, Martha Rianna, Lidia Puspita Sari Sagala, Nining S. Asri, Anggito Pringgo Tetuko, EkoArief Setiadi, Lukman Faris Nurdiyansah, Erwin Amiruddin, TimbangenSembiring, Perdamean Sebayang. 2022. Nano-structures and magnetic properties of Zn1-xCux/2Nix/2Fe2O4 (x =0-0.4) synthesized from natural iron sand. South African Journal of Chemical Engineering. 42, pp. 216-222.

[30] Erwin Amiruddin, Salomo Sinuraya, Rahmondia N. Septiadi, YanuarHamzah, Amir Awaluddin, Loly A. Hardani, Fitri A. Lestari, Yessi Magdalena and Devi T. Gurning. 2022. A Systematic Study of the Structural and MagneticProperties of Nickel Doped α-Fe_2O_3 nanoparticles Prepared from Logas Natural Sand. ARPN Journal of Engineering and Applied Sciences. 17(14): 1408-1413.

[31] Erwin Amiruddin and Adhy Prayitno. 2016. Transmission Electron Microscopy Study of Magnetic Domain of Cobalt-Samarium Thin Films Fabricated Using DC Magnetron Sputtering Technique. Kn Engineering. DOI 10.18502/keg.v1i1.503

[32] Martha Rianna, Marhaposan Situmorang, Candra Kurniawan, Anggito P. Tetuko, EkoArief Setiadi, MasnoGinting, Perdamean Sebayang. 2019. The effect of Mg-Al additive concentration on microstructure, magnetic properties, and microwave absorption on $BaFe_{12-2x}Mg_xAl_xO_{19}$(x = 0–0.5) material synthesized from natural iron sand. Materials Letters. 256, 126612. doi.org/10.1016/j.matlet.2019.126612

[33] Ahmed A.S., Shafeeq M.M., Singla M.L., Tabassum S., Naqvi A.H., Azam A., J. Lumin. 2010. 131, 1.

[34] Nina Popov, StjepkoKrehula, Mira Risti´c, Ern″ o Kuzmann, Zolt´an Homonnay, Marko Bo˘skovi´c, DaliborStankovi´c, ShiroKubuki, SvetozarMusi´c. 2021. Influence of Cr doping on the structural, magnetic, optical and photocatalytic properties of α-Fe2O3 nanorods. Journal of Physics and Chemistry of Solids: 148, 109699, pp. 1-12

[35] A.S. Teja, P.-Y. Koh. 2008. Synthesis, properties and applications of magnetic iron oxide nanoparticles. Progress in Crystal Growth and Characterization of Materials. 55, 22-45, DOI: 10.1016/ j.pcrysgrow. 2008.08.003.

[36] Prakash Chand, Anurag Gaur, Ashavani Kumar. 2014. Effect of Cr and Fe Doping on the Structural and Optical Properties of ZnO Nanostructures. World Academy of Science. Engineering and Technology

©2006-2023 Asian Research Publishing Network (ARPN). All rights reserved.

International Journal of Chemical and Molecular Engineering. 8(12): 1321-1324.

[37] Lassoued A, Dkhil B, Gadri A and Ammar S. 2017. Control of the shape and size of iron oxide (α-Fe_2O_3) nanoparticles synthesized through the chemical precipitation method Results Phys. pp. 73007-15.

[38] Asfandyar Khan, ZsoltValicsek and OttóHorváth. 2020. Synthesis, Characterization and Application of Iron (II) Doped Copper Ferrites ($Cu^{II}_{(x)}Fe^{II}_{(1-x)}Fe^{III}_2O_4$) as Novel Heterogeneous Photo-Fenton Catalysts. Nanomaterials: 10, 921; doi:10.3390/nano10050921

[39] Guo S., Zhang G., Jimmy C.Y. 2015. Enhanced photo-Fenton degradation of rhodamine B using grapheme oxide-amorphous $FePO_4$ as efective and stable heterogeneous catalyst. J. Colloid Interf. Sci. 448, 460-466.